Accepted Manuscript

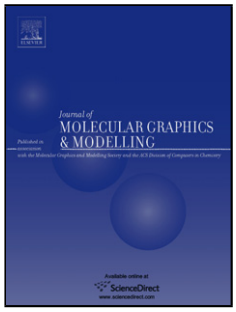

Title: Structural and Quantum Mechanical Computations to Elucidate the Altered Binding Mechanism of Metal and Drug with Pyrazinamidase from *Mycobacterium tuberculosis* due to Mutagenicity

Authors: Nouman Rasool, Saima Iftikhar, Waqar Hussain

PII: S1093-3263(17)30722-2
DOI: https://doi.org/10.1016/j.jmgm.2017.12.011
Reference: JMG 7086

To appear in: *Journal of Molecular Graphics and Modelling*

Received date: 20-9-2017
Revised date: 18-12-2017
Accepted date: 21-12-2017

Please cite this article as: Nouman Rasool, Saima Iftikhar, Waqar Hussain, Structural and Quantum Mechanical Computations to Elucidate the Altered Binding Mechanism of Metal and Drug with Pyrazinamidase from Mycobacterium tuberculosis due to Mutagenicity, Journal of Molecular Graphics and Modelling https://doi.org/10.1016/j.jmgm.2017.12.011

Structural and Quantum Mechanical Computations to Elucidate the Altered Binding Mechanism of Metal and Drug with Pyrazinamidase from *Mycobacterium tuberculosis* due to Mutagenicity

Short title: Quantum mechanics of mutagenicity in *Mycobacterium tuberculosis*

Nouman Rasool[1*], Saima Iftikhar[2], Waqar Hussain[3]

[1] Department of Life Sciences, University of Management and Technology, Lahore, Pakistan.

[2] School of Biological Sciences, University of the Punjab, Lahore, Pakistan.

[3] Department of Computer Sciences, University of Management and Technology, Lahore, Pakistan.

Email:

Nouman Rasool: nouman.rasool@umt.edu.pk

Saima Iftikhar: saima.sbs@pu.edu.pk

Waqar Hussain: umt.waqar@outlook.com

[*]Corresponding Author: nouman.rasool@umt.edu.pk

*Present Address: University of Management and Technology, C-II Johar Town, Lahore, Pakistan.

Graphical Abstract

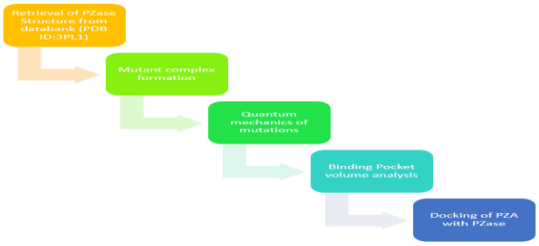

Highlights

- Pyrazinamidase, activator for pyrazinamide, leads to resistance against the drug due to mutagenicity across the world.
- In presents study, quantum mechanical calculations were performed to analyse the effect of mutations.
- Conformational changes in PZase binding cavity has also been analysed due to mutations of binding pocket residues.
- Iron showed weak binding with the metal coordination site of the mutant proteins.
- Binding cavity of the mutant PZase has undergone major conformational changes and reduce the drug activation mechanism leading to increased drug resistance in the bacterial strains.

Abstract

Pyrazinamide is known to be the most effective treatment against tuberculosis disease and is known to have bacteriostatic action. By targeting the bacterial spores, this drug reduces the chances for the progression of the infection in organisms. In recent years, increased instances of the drug resistance of bacterial strains are reported. Pyrazinamidase, activator for pyrazinamide, leads to resistance against the drug due to mutagenicity across the world. The present study aimed at the quantum mechanistic analysis of mutations in pyrazinamidase to gain insights into the mechanism of this enzyme. Quantum mechanical calculations were performed to analyse the effect of mutations at the metal coordination site using ORCA software program. Moreover, conformational changes in PZase binding cavity has also been analysed due to mutations of binding pocket residues using CASTp server. In order to elucidate the behaviour of the mutant pyrazinamidase, docking of PZA in the binding pocket of PZase was performed using AutoDock Vina. Analysis of results revealed that iron showed weak binding with the metal coordination site of the mutant proteins due to alteration in electron transfer mechanism. The binding cavity of the mutant PZase has undergone major conformational changes as the volume of pocket increased due to bulky R-chains of mutated amino acids. These conformational changes lead to weak binding of the drug at binding cavity of PZase and reduce the drug activation mechanism leading to increased drug resistance in the bacterial strains.

Keywords: *Mycobacterium tuberculosis*; Pyrazinamidase; Pyrazinamide; Mutagenicity; Quantum mechanics; DFT; Molecular docking;

Introduction

Tuberculosis disease is one of the major concerns of the being faced by the world, as about one third of the population is suffering from this infection (Onyango, 2011). The disease is caused

by an obligate pathogenic bacterial species *Mycobacterium tuberculosis* from the family *Mycobacteriaceae.* There is an unusual waxy coating present at the cell surface of *Mycobacterium tuberculosis,* primarily due to the mycolic acid. Permeability to gram staining reduces due to mycolic acid coating and as a result, *Mycobacterium tuberculosis* appears either as gram positive or gram negative bacteria (McQuade *et al*., 2011). Pyrazinamide (PZA) is the first-line drug which is used as a short course treatment against tuberculosis. It reduces the duration of antituberculous treatment due to its mechanism against persistence of tubercle bacilli at an acidic pH (Heifets and Cangelosi, 1999). PZA metabolizes into its active form pyrazinoic acid (POA) due to the amidase activity of pyrazinamidase (PZase). This enzyme is encoded by *pncA* gene and the mutations in this enzyme lead to PZA resistance in *Mycobacterium tuberculosis* (Dooley *et al*., 2012). The mutations in PZase are diverse in nature and the drug resistance of bacteria enhances due to mutagenicity of PZase (Dhiman *et al*., 2013). Multi drug resistant tuberculosis (MDR-TB) is caused due to the resistance of two or more first line drugs. Therefore, various strategies are being adapted to find drugs against such complex disease.

Various mutations have been identified in PZase which makes this enzyme more drug resistant to drug therapies (Dooley *et al*., 2012; Dhanjal *et al*., 2014). The non-synonymous mutations in PZase leads to the loss of PZA activity. Metal coordination site (MCS) and catalytic site, both are known to play pivotal role in the enzymatic activity of protein. MCS is necessary for the activity of PZase, as it is a metalloenzyme and contains iron as a cofactor. The iron ion of PZase coordinates with a tetrad of amino acids, comprising of one aspartic acid and three histidine residues (Khadem-Maaref *et al*., 2017). Moreover, the metal is coordinated with two water molecules as well. Metal substitution at MCS can also alter the activity of this enzyme, however, mutations play more fundamental role in the drug resistance of PZase. The diverse nature of mutations is the most prominent characteristic as the mutations range from missense

mutations to insertion/deletion mutations (Vats *et al*., 2015). The modification of PZA to POA is acidic which makes it cumbersome to analyse the drug resistance of *Mycobacterium tuberculosis*, reliably. PCR amplification and DNA sequencing is a well-known technique for rapid identification of mutations, however, such analysis can be costly and laborious. In contrast, the computational analysis of such mutations can elucidate the effect of mutagenicity of PZase as *in silico* studies narrow down the investment of time, effort and cost. *In silico* analysis can be considered as a pre-process of experimental studies because it minimizes number of cases to be considered. The docking of inhibitors with the enzymes elucidate the mechanism of inhibition along with the specificity and efficiency of that inhibitor. Density functional theory is a computational approach for quantum mechanical calculations and is currently being used in biological systems. The calculations within the system are based on various exchange correlations i.e. Perdew and Wang (PW), Becke (B and B3) and the Lee, Yang and Parr (LYP) (Orio *et al*., 2009). These are more the commonly used functional. B3LYP incorporate a portion of exact exchange from Hartree–Fock theory with exchange and correlation from other sources such as generalized gradient approximations from Becke88 and Lee-Yang-Parr (Gill *et al*., 1992). However, PWP and BP86 are linear approximations. Analysis of chemical reactivity descriptors using DFT is very important to understand chemical and biological activities of the compounds against the biological target. It helps in characterizing the electrophilic or nucleophilic nature, their ionization, potential and affinity towards the targets (Minenkov *et al*., 2012).

The present study aims at the quantum mechanistic analysis of mutant PZase complexes by studying the mechanics of metal and PZA at MCS and binding cavity, respectively. It was primarily targeted to understand the quantum mechanism of drug resistance of PZase at molecular level by analysing structural and mechanical properties of PZase. A total of 12 mutant complexes are considered in this study to elucidate the effect of mutations on the

enzymatic function of PZase. Through results, it is observed that the mutations can lead to major conformational changes in the tertiary structure of protein, specifically the binding cavity which leads to loose binding of PZA with PZase.

Material and Methods

Computational analysis of mutations in PZase (listed in Table 1) is performed in this study. The structure of PZase (PDB ID: 3PL1) was retrieved from protein databank (Figure 1). As revealed by X-ray crystallography, the protein is composed of 185 amino acid residues. The α/β domain is formed by four α –helices and six β-sheets. Through site directed mutagenesis, it has been revealed that Asp_8, Lys_{96} and Cys_{138} play a pivotal role in catalysis; and Asp_{49}, $His_{51,}$ His_{57} and His_{71} are the metal ion binding residues (Petrella *et al*., 2011). A total of 12 mutant protein-metal complexes of PZase were generated using mutagenesis package in PyMol (Delano, 2002).

Mechanics of mutations in PZase

The quantum mechanical calculations of native PZase and all the 12 mutant complexes were performed in ORCA version 3.0.1 package (Neese *et al*., 2012). The quantum mechanical calculation included, molecular geometry optimization and single point energy calculations with different density functional theory correlations i.e. B3LYP, PWP and BP86. Entire protein calculations were performed for geometry optimization using def2-SV(P) basis set. After the optimization, four MCS residues; FE^{2+} and two coordinated water molecules were targeted for energy calculations to analyse the effect of mutations at metal binding mechanism of PZase Generally, the hybrid exchange correlation is a combination of Hartree-Fock exact exchange functional and any other density functional. However, the targeted correlation i.e. B3LYP is defined as:

$$E_{xc}^{B3LYP} = E_x^{LDA} + a_0 (E_x^{HF} - E_x^{LDA}) + a_x (E_x^{GGA} - E_x^{LDA}) + E_c^{LDA} + a_c (E_c^{GGA} - E_c^{LDA})$$

Where $a_0 = 0.20$, $a_x = 0.72$, and $a_c = 0.81$. E_x^{GGA} is actually the generalized gradient approximation for the Becke 88 functional while the E_c^{GGA} reflects the correlation functional of Lee-Yang-Parr. With this hybrid functional, local density approximation is added in the form of E_c^{LDA}. PWP and BP86 are linear and gradient-corrected correlation functional. The complexes were optimized in aqueous phase using conductor like screening model (COSMO) (Sinnecker *et al*., 2006). The ChelpG method was adapted to calculate the equivalent charges on all the atoms from the mutant complexes (Breneman *et al*., 1990).

Binding pocket analysis

Computed atlas of surface topography of proteins (CASTp) server was used for the analysis of conformational changes in the binding pocket. CASTp used weighted Delaunay triangulation and alpha complex for shape measurements and generated information about volume and area of the binding pocket of each (Binkowski *et al*., 2003).

Molecular docking and Binding energy estimation

The docking study was performed to analyse the interaction of PZA with PZase. The ligand and protein preparation was performed in AutoDock Tools and docking was performed using AutoDock Vina (Morris *et al*., 2009; Trott and Olson, 2010). The interactions of the PZA was analysed along with the estimation of binding energies using Autodock Vina. For further analysis of docking, K_i was calculated by the equation:

$$K_i = e^{\frac{\Delta G}{R \times T}},$$

Where ΔG is docking energy, R (gas constant) is 1.9872036 cal/mol and T (temperature) is 298.15K.

Analysing reactivity of PZA in the binding pocket of PZase

A DFT-based analysis was carried out using ORCA program to study the reactivity of PZA in the binding pocket of PZase. For each PZase-PZA complex, PZA along with the interacting residues was subjected to DFT calculations. Both the orbital based descriptors i.e. Highest Occupied Molecular Orbital (HOMO) and Lowest Unoccupied Molecular Orbital (LUMO) energies were calculated by applying the B3LYP hybrid functional exchange correlation of DFT (Becke *et al*., 1993). Adopting this hybrid approach, molecular orbital energies were calculated and band energy gap (ΔE) was analysed using the expression E_{LUMO}-E_{HOMO} adapting the def2-SV(P) basis set.

Results and Discussion

The conventional therapies for the tuberculosis disease are being affected by the continuously emerging mutations in *Mycobacterium tuberculosis*. Among various mutations occurring in PZase, some mutations do not alter the activity of enzyme while other cast drastic effect on the enzymatic activity of PZase. Mutations occurring at substrate binding site and MCS has deleterious effect on enzyme activity (Sheen *et al*., 2012). The mechanism of drug resistance due to the mutations at MCS and catalytic site is necessary to be analysed, therefore, the present study aimed at the *in silico* analysis of such mutations through quantum mechanics and their impact on the activity of PZase.

Metal to ligand bond lengths

While analysing the mutated complexes, it was observed that metal to ligand bond lengths varied in only those complexes which had mutations in MCS or close to MCS (Figure 2).

The complexes with mutations Asp_{49} → Asn, His_{51} → Gln, His_{57} → Asp, Ser_{67} → Pro and Gly_{78} → Cys showed a significant variation in the metal to ligand bond lengths. No significant variation in metal to ligand bond length was observed in the complexes when mutations

occurred at active site or close to active site (Table 2). For Comp-0, the bond lengths ranged within 2.118Å to 2.244Å. For Comp-4, the bond lengths ranged within 2.101Å to 2.234Å and for Comp-5, the bond length ranged within 2.103Å to 2.235Å. Similarly, the bond lengths ranged within 2.101Å to 2.234 and 2.011Å to 2.239Å for Comp-6 and Comp-7, respectively. Moreover, significant difference was observed in Comp-8 as the bond lengths ranged within 2.112Å to 2.246Å. Due to mutation at MCS, the bonding of iron varied as iron made no bond with the mutated residues i.e. Asp_{49} → Asn, His_{51} → Gln and His_{57} → Asp. Among all the MCS residues, Asp_{49} is known to be actively bound with the iron. It is previously reported that due to mutation of Asp_{49} →Asn, the change in polarity resulted in termination of bond with iron (Jureen *et al*., 2008; Petrella *et al*., 2011).

Partial charges in aqueous phase

Due to substantial variation in the metal to ligand bond length in Comp-4, Comp-5, Comp-6, Comp-7 and Comp-8, the electron transfer mechanism was analysed for only these complexes and compared with non-mutated complex i.e. Comp-0. The electrons were transferred from MCS residues and water molecules towards metals, which represented the partial charges (Table 3).

The trend of partial charges remained same for all the MCS residues, water molecules and metal, except the mutant residues. In Comp-4, variation in charges was due to mutation of Asp_{49} →Asn as aspartic acid is a negatively charged amino acid and was mutated with asparagine, a positively charged amino acid. Such variation in the charges of amino acid effected electron transfer mechanism of MCS towards metal. In Comp-6, His_{57} → Asp mutation caused substantial changes in partial charges as a positively charged residue i.e.

histidine was mutated with aspartic acid which is negatively charged. For Comp-5, His_{51} was mutated with glutamine and both are positively charged residues, therefore the partial charges were slightly changed. Since the electronic charge shifts from the molecular orbital with the ligand to the metal, these complexes are known as ligand-to-metal charge-transfer (LMCT) complexes. Metal to ligand lengths are varied due to the change in mechanism of electron transfer which elucidates that the metal to ligand bond lengths depend on the partial charges as well (Nemethy *et al*., 1983; Khadem-Maaref *et al*., 2017).

Dipole moment of iron coordinated water molecules

Metal to ligand bond polarity was measured using dipole moment which showed the difference of charge in the chemical bonds of iron with MCS residues and water. The dipole moment of metal coordinated water molecules was also analysed for Comp-4, Comp-5, Comp-6, Comp-7 and Comp-8 and compared with non-mutated complex i.e. Comp-0 (Table 4).

The values ranged within 2.90 Debye to 2.94 Debye. The order of dipole moment in different complexes was Comp-0 (2.94 Debye) > Comp-4 (2.93 Debye) > Comp-8 (2.92 Debye) > Comp-5 (2.91 Debye) > Comp-7 (2.91 Debye) > Comp-6 (2.90 Debye). The major changes in dipole moment of Comp-4, Comp-5 and Comp-6 were due to absence of bonds with the mutated residues at MCS. Dipole moment is directly associated with bond length as it is the magnitude of the charge at either end of the chemical bond or molecule dipole multiplied by the distance between the charges (Biro *et al*., 2006). As in result of mutations, iron induced different polarizations on the iron-water bonds and affected the iron binding and PZase activity. The variation in the side chain lead to variation in the bond polarization mechanism of iron. The coordinated water polarization can facilitate the deprotonating event that plays an

important role in the enzymatic reaction of PZase (Petrella *et al*., 2011; Khadem-Maaref *et al*., 2017).

Binding of iron with mutated complexes

DFT based single point energies helped in measuring the iron binding energies within the MCS of PZase in each mutated complex. The difference between the hydration and complexation energies of the enzyme-iron complex was calculated to identify the ability of iron binding in the mutated MCS (Table 5). Complexation energy was calculated as iron + PZase and the hydration energy was calculated using iron + 6 H_2O molecules. The difference of both energies determined the protienation energy which was predicted using the PWP, BP86, and B3LYP exchange correlation functionals (Figure 3).

B3LYP and BP86, both exchange correlations showed same behaviour for binding energies as the energies decreased in order of Comp-0>Comp-8>Comp-7>Comp-5>Comp-4>Comp-6. A variation in order was observed by applying PWP correlation functional i.e. Comp-0>Comp-8>Comp-7>Comp-5> Comp-6>Comp-4 due to the non-hybrid behaviour of this correlation functional (Becke *et al*., 1993). Iron tightly bound with the wild type PZase, therefore the binding energy released was maximum. In mutant complexes, it was observed that iron made no bonds with the mutant residues. Due to this, bonding of iron with mutants was weak as compared to that of with wild type PZase. The decreased binding energy in mutant complexes result in decreased catalytic activity leading to decreased binding of PZA, and these results are also in accordance with previously reported studies (Jureen *et al*., 2008; Dudley *et al*., 2016).

Binding cavity analysis

Binding pocket analysis is important to identify the impact of mutation at the binding pocket. The volume of the binding pocket for native PZase was 551.9 $Å^3$ and a considerable difference is observed in the binding pocket volume of mutants, having mutation in active site residues or close to that site i.e. Comp-1, Comp-2, Comp-11 and Comp-12 (Table 6).

In Comp-1 and Comp-2, Asp_{12} was mutated with glycine and alanine, respectively. The binding pocket volume of Comp-1 (733.2 $Å^3$) was less as compared to Comp-2 (1113.8 $Å^3$) because size of glycine is less than alanine (Biro *et al*., 2006). In Comp-11, Thr_{135} → Pro mutation increased the volume of pocket i.e. 551.9 $Å^3$ to 1442.1.7 $Å^3$, as the Epstein's coefficient of difference is higher for these both amino acids i.e. 0.8 out of 1 (Epstein, 1967). The volume of binding pocket also increased in Comp-12 having Cys_{138} → Tyr mutation i.e. from 551.9 $Å^3$ to 834.7 $Å^{3.}$ It was less as compared to that of Comp-2 and Comp-11 due to less score of Epstein's coefficient of difference between cystine and tyrosine i.e. 0.25 out of 1 (Epstein, 1967). The increase in volume affects the binding of PZA within active cavity thereby decreasing the stability of the ligand at the pocket and reducing the catalytic process (Vats *et al*., 2015). In order to further evaluate the behaviour of the mutant, docking was performed.

Binding of PZA with PZase and reactivity of PZA

For a thorough analysis of mutations in PZase, PZA was docked with all the mutant complexes. Binding affinities of PZA against PZase ranged within Maximum binding affinity was observed with wild type PZase i.e. -4.7 kcal/mol. A mutant Comp-8 also exhibited same binding affinity of PZA with PZase i.e. -4.7 kcal/mol as the mutation in Comp-8 was not near to active site. In remaining complexes, the binding of PZA with PZase was weaker than that of wild type PZase due to increase in the binding pocket volume (Table 7).

Residues involved in the interactions with PZA were Asp_{8}, Phe_{13}, Leu_{19}, Val_{21}, Ile_{133}, His_{137}, Cys_{138} and Val_{163}. For further analysis, DFT based analysis was carried out to calculate the band energy gap i.e. difference of HOMO and LUMO energies. The band energy gap ranged within 0.230 eV to 0.321 eV and the lowest score reflected higher reactivity (Table 8). Reactivity of PZA was highest in the binding pocket of wild type PZase due to less conformational changes in the binding pocket. All the three factors i.e. volume of binding pocket, docking score and reactivity, typically used here to explain the reason for resistance to drug supported the idea of weak binding of the ligand with the protein in mutated form, which was hampering its activation (Vats *et al*., 2015; Dudley *et al*., 2016).

The increased volume of binding pocket reveals that PZA will loosely bind with the catalytic site of PZase. The acidic modification of PZA to POA depends on the strength of its binding with PZase. Weak binding will cause less acidic modification which is not an optimum condition for treatment. As per the docking and band energy gaps analysis, it is observed that reactivity of PZA also decreases within the binding cavity of PZase. The mutagenicity is increasing the drug resistant nature of PZase by altering the drug and metal binding mechanism of PZase (Jureen *et al*., 2008).

Conclusion

The present study elucidated the effect of mutations in the enzymatic functions of PZase. A total of 12 mutations were performed in the PZase which were at active site, metal coordination site and residues close to them. Some mutations were distant from both these sites and did not cause any deleterious effect on the structure and function of PZase. Based on results, it is

concluded that the mutations related to MCS and its close residues effect the metal binding with protein and cause weak bindings due to the difference in electron transfer mechanism of different residues. Moreover, it is observed that the mutations in the binding pocket residues lead to the major conformational changes in pocket, specifically increase in volume of binding pocket due to mutations Asp_{12} → Gly, Asp_{12} → Ala, Thr_{135} → Pro and Cys_{138} → Tyr. The pocket size increases and the binding of PZA with PZase becomes weaker as compared to binding with wild-type PZase. Weak binding of PZA causes less acidic modification and the mutagenicity of PZase leads to increased drug resistant nature of PZase. The analysis of PZase mutagenicity illustrates the susceptibility of PZA in *M. tuberculosis*. The affectivity and reactivity of the drug also reduces as per the band energy gap analysis. This causes less drug efficacy towards the tuberculosis. It is concluded that mutations in the PZase are major reason for drug resistant nature of this protein.

References

Becke, A. D. (1993). A new mixing of Hartree–Fock and local density-functional theories. *The Journal of chemical physics*, *98*(2), 1372-1377.

Billingsley, K. M., Smith, N., Shirley, R., Achieng, L., & Keiser, P. (2011). A quality assessment tool for tuberculosis control activities in resource limited settings. *Tuberculosis*, *91*, S49-S53.

Binkowski, T. A., Naghibzadeh, S., & Liang, J. (2003). CASTp: computed atlas of surface topography of proteins. *Nucleic acids research*, *31*(13), 3352-3355.

Biro, J. C. (2006). Amino acid size, charge, hydropathy indices and matrices for protein structure analysis. *Theoretical Biology and Medical Modelling*, *3*(1), 15.

Breneman, C. M., & Wiberg, K. B. (1990). Determining atom-centered monopoles from molecular electrostatic potentials. The need for high sampling density in formamide conformational analysis. *Journal of Computational Chemistry*, *11*(3), 361-373.

DeLano, W. L. (2002). PyMOL.

Dhanjal, J. K., Grover, S., Sharma, S., Singh, A. K., & Grover, A. (2014). Structural insights into mode of actions of novel natural Mycobacterium protein tyrosine phosphatase B inhibitors. *BMC genomics*, *15*(1), S3.

Dhiman, H., Dhanjal, J. K., Sharma, S., Chacko, S., Grover, S., & Grover, A. (2013). Resisting resistant Mycobacterium tuberculosis naturally: Mechanistic insights into the inhibition of the parasite's sole signal peptidase Leader peptidase B. *Biochemical and biophysical research communications*, *433*(4), 552-557.

Dooley, K. E., Mitnick, C. D., Ann DeGroote, M., Obuku, E., Belitsky, V., Hamilton, C. D., & Nuermberger, E. (2012). Old drugs, new purpose: retooling existing drugs for optimized treatment of resistant tuberculosis. *Clinical Infectious Diseases*, *55*(4), 572-581.

Dudley, M. Z., Sheen, P., Gilman, R. H., Ticona, E., Friedland, J. S., Kirwan, D. E., & Grandjean, L. (2016). Detecting Mutations in the Mycobacterium tuberculosis Pyrazinamidase Gene pncA to Improve Infection Control and Decrease Drug Resistance Rates in Human Immunodeficiency Virus Coinfection. *The American journal of tropical medicine and hygiene*, *95*(6), 1239-1246.

Epstein, C. J. (1967). Non-randomness of Ammo-acid Changes in the Evolution of Homologous Proteins. *Nature*, *215*(5099), 355-359.

Heifets, L. B., & Cangelosi, G. A. (1999). Drug susceptibility testing of Mycobacterium tuberculosis: A neglected problem at the turn of the century [State of the Art]. *The international journal of tuberculosis and lung disease*, *3*(7), 564-581.

Juréen, P., Werngren, J., Toro, J. C., & Hoffner, S. (2008). Pyrazinamide resistance and pncA gene mutations in Mycobacterium tuberculosis. *Antimicrobial agents and chemotherapy*, *52*(5), 1852-1854.

Khadem-Maaref, M., Mehrnejad, F., & Phirouznia, A. (2017). Effects of metal-ion replacement on pyrazinamidase activity: A quantum mechanical study. *Journal of Molecular Graphics and Modelling*, *73*, 24-29.

Minenkov, Y., Singstad, Å., Occhipinti, G., & Jensen, V. R. (2012). The accuracy of DFT-optimized geometries of functional transition metal compounds: a validation study of catalysts for olefin metathesis and other reactions in the homogeneous phase. *Dalton Transactions*, *41*(18), 5526-5541.

Morris, G. M., Huey, R., Lindstrom, W., Sanner, M. F., Belew, R. K., Goodsell, D. S., & Olson, A. J. (2009). AutoDock4 and AutoDockTools4: Automated docking with selective receptor flexibility. *Journal of computational chemistry*, *30*(16), 2785-2791.

Neese, F. (2012). The ORCA program system. *Wiley Interdisciplinary Reviews: Computational Molecular Science*, *2*(1), 73-78.

Nemethy, G., Pottle, M. S., & Scheraga, H. A. (1983). Energy parameters in polypeptides. 9. Updating of geometrical parameters, nonbonded interactions, and hydrogen bond interactions for the naturally occurring amino acids. *The Journal of Physical Chemistry*, *87*(11), 1883-1887.

Onyango, R. O. (2011). State of the globe: Tracking tuberculosis is the test of time. *Journal of global infectious diseases*, *3*(1), 1.

Orio, M., Pantazis, D. A., & Neese, F. (2009). Density functional theory. *Photosynthesis research*, *102*(2-3), 443-453.

Petrella, S., Gelus-Ziental, N., Maudry, A., Laurans, C., Boudjelloul, R., & Sougakoff, W. (2011). Crystal structure of the pyrazinamidase of Mycobacterium tuberculosis: insights into natural and acquired resistance to pyrazinamide. *PLoS One*, *6*(1), e15785.

Sheen, P., Ferrer, P., Gilman, R. H., Christiansen, G., Moreno-Román, P., Gutiérrez, A. H., & Flores, M. (2012). Role of metal ions on the activity of Mycobacterium tuberculosis pyrazinamidase. *The American journal of tropical medicine and hygiene*, *87*(1), 153-161.

Sinnecker, S., Rajendran, A., Klamt, A., Diedenhofen, M., & Neese, F. (2006). Calculation of solvent shifts on electronic g-tensors with the conductor-like screening model (COSMO) and its self-consistent generalization to real solvents (Direct COSMO-RS). *The Journal of Physical Chemistry A*, *110*(6), 2235-2245.

Trott, O., & Olson, A. J. (2010). AutoDock Vina: improving the speed and accuracy of docking with a new scoring function, efficient optimization, and multithreading. *Journal of computational chemistry*, *31*(2), 455-461.

Vats, C., Dhanjal, J. K., Goyal, S., Gupta, A., Bharadvaja, N., & Grover, A. (2015). Mechanistic analysis elucidating the relationship between Lys96 mutation in Mycobacterium tuberculosis pyrazinamidase enzyme and pyrazinamide susceptibility. *BMC genomics* (Vol. 16, No. Suppl 2, p. S14). BioMed Central Ltd.

Figures

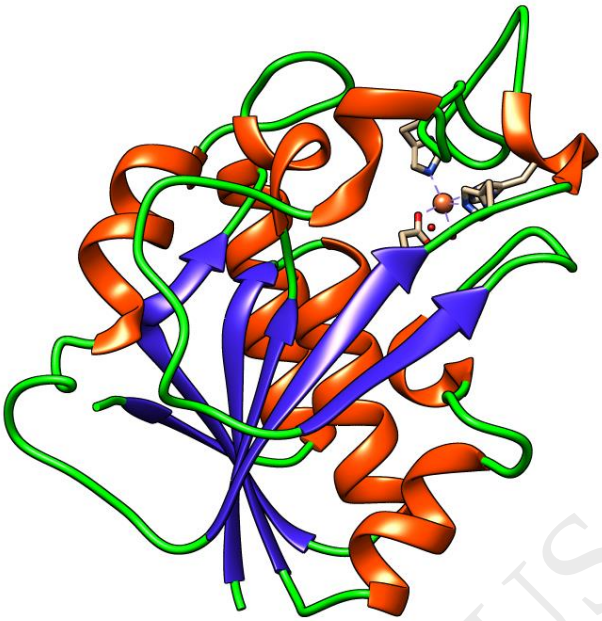

Figure 1: Tertiary structure of pyrazinamidase from *Mycobacterium tuberculosis* (PDB ID: 3PL1)

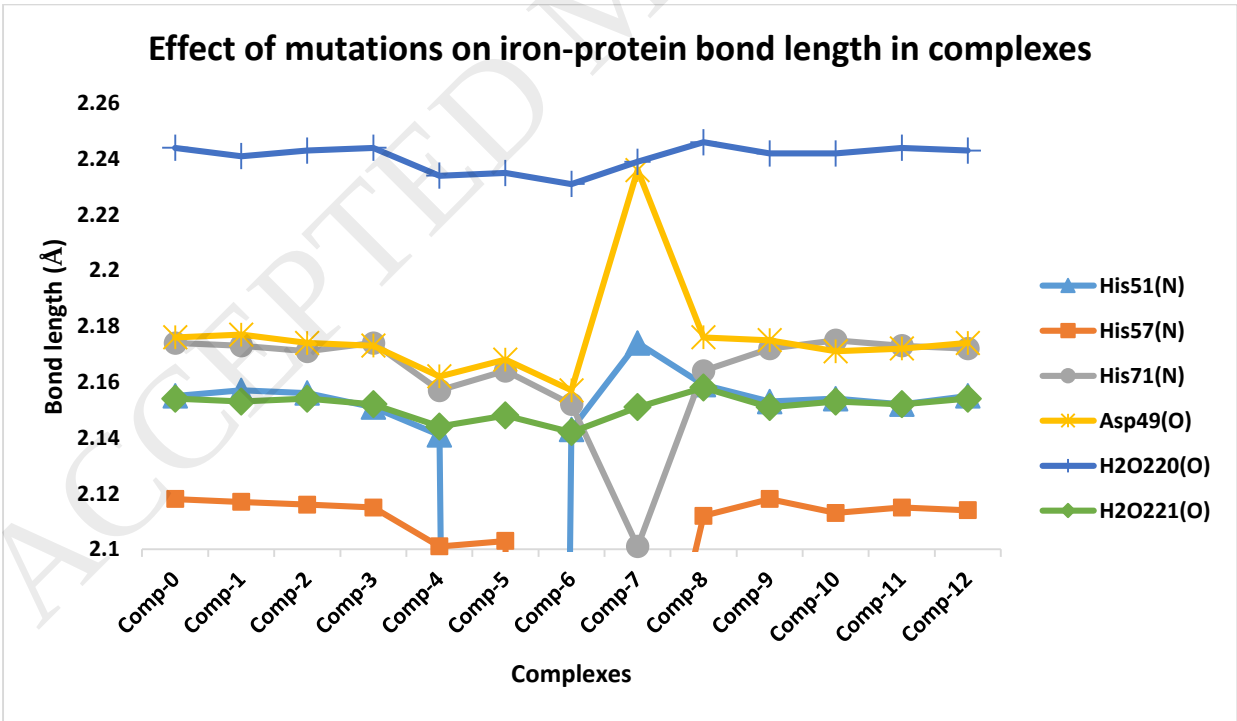

Figure 2: Effect of mutations on iron-protein bond length in complexes

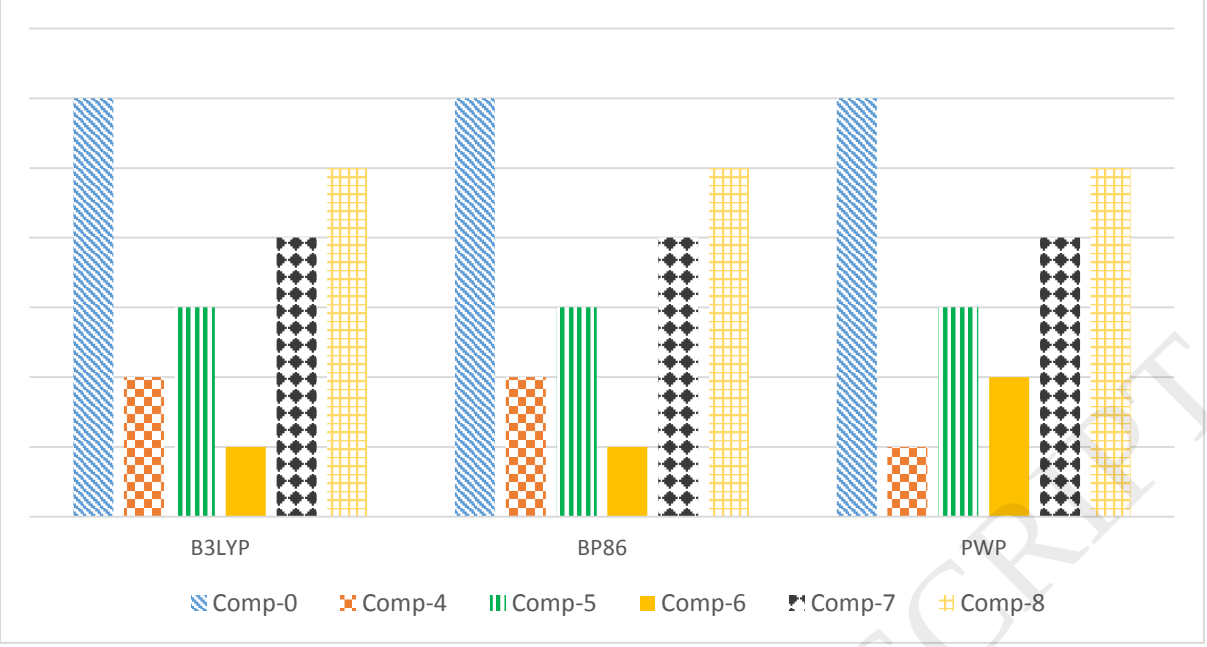

Figure 3: Proteination energies computed using B3LYP, BP86 and PWP exchange correlation functionals

Tables

Table 1: Complexes used in this study

Complex	**Mutation**	**Type**
Comp-0	*No mutation*	
Comp-1	Asp_{12} → Gly	Close to both MCS and Active site
Comp-2	Asp_{12} → Ala	Close to both MCS and Active site
Comp-3	Gly_{24} → Asp	Distant residues from MCS and Active site
Comp-4	Asp_{49} → Asn	MCS residue
Comp-5	His_{51} → Gln	MCS residue
Comp-6	His_{57} → Asp	MCS residue
Comp-7	Ser_{67} → Pro	Close to MCS
Comp-8	Gly_{78} → Cys	Close to MCS
Comp-9	Phe_{94} → Leu	Distant residues from MCS and Active site
Comp-10	Leu_{116} → Pro	Distant residues from MCS and Active site
Comp-11	Thr_{135} → Pro	Close to active site
Comp-12	Cys_{138} → Tyr	Active site residue

Table 2: Ordering of the iron-ligand bond lengths by incorporating mutations (Å)

Complex	**His_{51}(N)**	**His_{57}(N)**	**His_{71}(N)**	**Asp_{49}(O)**	**H_2O220(O)**	**H_2O221(O)**
Comp-0	2.155	2.118	2.174	2.176	2.244	2.154
Comp-1	2.157	2.117	2.173	2.177	2.241	2.153
Comp-2	2.156	2.116	2.171	2.174	2.243	2.154
Comp-3	2.151	2.115	2.174	2.173	2.244	2.152
Comp-4	2.141	2.101	2.157	-	2.234	2.144
Comp-5	-	2.103	2.164	2.168	2.235	2.148
Comp-6	2.143	-	2.152	2.157	2.231	2.142
Comp-7	2.174	2.011	2.101	2.236	2.239	2.151
Comp-8	2.159	2.112	2.164	2.176	2.246	2.158
Comp-9	2.153	2.118	2.172	2.175	2.242	2.151
Comp-10	2.154	2.113	2.175	2.171	2.242	2.153
Comp-11	2.152	2.115	2.173	2.172	2.244	2.152
Comp-12	2.155	2.114	2.172	2.174	2.243	2.154

Table 3: Partial charges in aqueous phase (au)

Complex	Comp-0	Comp-4	Comp-5	Comp-6	Comp-7	Comp-8
Fe2+	0.9118	0.9021	0.8997	0.9034	0.9102	0.9088
His51(N)	−0.2016	−0.2002	−0.1999	−0.2005	−0.2013	−0.2011
His57(N)	-0.2061	-0.2013	-0.2002	-0.1775	-0.2053	-0.2048
His71(N)	-0.3735	-0.3709	-0.3698	-0.3702	-0.3726	-0.3722
Asp49(O)	-0.7306	-0.6212	-0.7247	-0.7279	-0.7301	-0.7299
H2O220(O)	-0.9193	-0.9122	-0.9109	-0.9134	-0.918	-0.9173
H2O220(H)	0.5219	0.5201	0.5176	0.5198	0.5208	0.5205
H2O220(H)	0.484	0.4829	0.4799	0.4814	0.4837	0.4833
H2O221(O)	-1.0496	-1.0425	-1.0411	-1.0437	-1.0481	-1.0475
H2O221(H)	0.5954	0.5911	0.5899	0.5922	0.5948	0.5939
H2O221(H)	0.5099	0.5029	0.5008	0.5047	0.5087	0.5085

Table 4: Dipole moment of iron coordinated water molecules (Debye)

Complex	H_2O(220)	H_2O(221)	Average
Comp-0	2.82	3.06	2.94
Comp-4	2.81	3.04	2.93
Comp-5	2.80	3.01	2.91
Comp-6	2.79	3.00	2.90
Comp-7	2.80	3.02	2.91
Comp-8	2.81	3.03	2.92

Table 5: Order of Iron binding energies with different exchange correlation functionals

Energy Function	Order
Hydration	
B3LYP	Comp-0>Comp-8>Comp-7>Comp-5>Comp-4>Comp-6
BP86	Comp-0>Comp-8>Comp-7>Comp-5>Comp-4>Comp-6
PWP	Comp-0>Comp-8>Comp-7>Comp-5>Comp-6>Comp-4
Complexation	
B3LYP	Comp-0>Comp-8>Comp-7>Comp-5>Comp-4>Comp-6
BP86	Comp-0>Comp-8>Comp-7>Comp-5>Comp-4>Comp-6
PWP	Comp-0>Comp-8>Comp-7>Comp-5>Comp-4>Comp-6
Proteination	
B3LYP	Comp-0>Comp-8>Comp-7>Comp-5>Comp-4>Comp-6
BP86	Comp-0>Comp-8>Comp-7>Comp-5>Comp-4>Comp-6
PWP	Comp-0>Comp-8>Comp-7>Comp-5>Comp-6>Comp-4

Table 6: Binding cavity volume analysis

Complex	Volume of binding pocket ($Å^3$)
Comp-0	551.9
Comp-1	733.2
Comp-2	1113.8
Comp-3	551.9
Comp-4	567.3
Comp-5	589.2
Comp-6	555.4
Comp-7	560.2
Comp-8	563.6
Comp-9	551.9
Comp-10	551.9
Comp-11	1442.1
Comp-12	834.7

Table 7: Binding free energy and K_i (μM) of pyrazinamide against pyrazinamidase

Complex	Interacting Residues	ΔG (kcal/mol)	K_i (μM)
Comp-0	Asp_8, Phe_{13}, Leu_{19}, Val_{21}, Ile_{133}, His_{137}, Cys_{138}, Val_{163}	-4.7	355.674
Comp-1	Leu_{19}, Val_{21}, Ile_{133}, His_{137}, Cys_{138}	-2.7	699.165
Comp-2	Ile_{133}, His_{137}, Cys_{138}, Val_{163}	-2.6	10439.733
Comp-3	Asp_8, Phe_{13}, Leu_{19}, Val_{21}, His_{137}	-4.2	12361.502
Comp-4	Asp_8, Phe_{13}, Leu_{19}, Val_{21}, Ile_{133}	-3.9	827.868
Comp-5	Asp_8, Leu_{19}, His_{137}, Cys_{138}, Val_{163}	-3.8	1374.380
Comp-6	Asp_8, Phe_{13}, Leu_{19}, Val_{21}, Val_{163}	-4.0	1627.379
Comp-7	Phe_{13}, Leu_{19}, His_{137}, Cys_{138}, Val_{163}	-3.7	1160.713
Comp-8	Asp_8, Phe_{13}, Leu_{19}, Cys_{138}, Val_{163}	-4.7	355.674
Comp-9	Asp_8, Phe_{13}, Leu_{19}, His_{137}, Cys_{138}, Val_{163}	-4.0	1627.379
Comp-10	Asp_8, Phe_{13}, Leu_{19}, Val_{21}, Ile_{133}, His_{137},	-4.1	1160.713
Comp-11	Phe_{13}, Leu_{19}, Val_{21}, Ile_{133}	-2.8	980.264
Comp-12	Asp_8, Phe_{13}, Leu_{19}, Val_{21}, Val_{163}	-3.7	1160.713

Table 8: Band energy gaps of PZA binding with PZase

Complex	**E_{LUMO} (kcal/mol)**	**E_{HOMO} (kcal/mol)**	**Band energy gap (ΔE)**
Comp-0	-0.222	-0.452	0.230
Comp-1	-0.261	-0.572	0.301
Comp-2	-0.270	-0.580	0.310
Comp-3	-0.229	-0.461	0.232
Comp-4	-0.240	-0.484	0.244
Comp-5	-0.241	-0.490	0.249
Comp-6	-0.233	-0.470	0.237
Comp-7	-0.255	-0.516	0.261
Comp-8	-0.222	-0.452	0.230
Comp-9	-0.233	-0.470	0.237
Comp-10	-0.230	-0.464	0.234
Comp-11	-0.260	-0.550	0.290
Comp-12	-0.281	-0.602	0.321